

New Type of Bridge Fault Current Limiter with Reduced Power Losses for Transient Stability Improvement of DFIG Wind Farm

D. Baimel, N. R. Chowdhury, J. Belikov, Y. Levron

***Abstract*—The paper presents a new active diode bridge fault current limiter (FCL) topology, and compares it to the classic diode bridge, Series Dynamic Breaking Resistor (SDBR), and active diode bridge FCL circuits. The comparison is done using a benchmark system that includes a 9 MW wind turbine with a doubly fed induction generator (DFIG), two 50 MW synchronous generators, and three step-up transformers. The results show that all three FCLs improve transient stability by limiting the currents peak, terminal voltage drop, active and reactive powers, and torque transients.**

***Keywords*—doubly fed induction generator, transient stability, fault ride through enhancement, fault current limiter.**

I. Introduction

DOUBLY fed induction generators (DFIG) that are typically used in wind turbines are very sensitive to grid faults. Since faults may result in dangerous high currents in the rotor circuit and converters, the generator has to be disconnected from the system by circuit breakers [1]. However, in order to keep the generator connected to the grid for as long as possible, Fault Current Limiters (FCL) may be used [2]. Such circuits limit the short circuit current but does not disconnect the generator from the grid. As a result, FCLs allow to reduce the fault current threshold, provide enhanced fault ride through capabilities for the wind turbine, and improve the transient stability of the power system. FCLs implement a varying impedance, which is connected in series to the device being protected. The impedance is very low during normal operation to minimize the power loss. However, during a fault, the impedance rises rapidly and limits the fault current. FCLs can be divided into two main groups—superconducting [3], [4] and non-superconducting [5]. The main advantages of the non-superconducting group are smaller size and weight, simpler structure, and low prices. Naturally, the main disadvantage is higher power losses. The most widespread types of superconducting FCLs are resistive [6], [7], [8] and inductive [9], [10], superconducting magnetic energy storage (SMES) [11], [12], and bridge-type FCLs [13]. The common topologies of non-superconducting FCLs are resistive such as series dynamic braking resistor (SDBR) [14], [15] and bridge type FCLs [13], [16], [17], [18], [19], [20], [21], [22], [23], [24], [25]. Typically, the bridge-type FCLs are comprised of passive (diodes) [13], [16], [17] or active (thyristors, MOSFETs, IGBTs) [26]. Additionally, there are also modified topologies such as bridge saturated core fault current limiter [27] and bridge-type solid-state fault current limiter that are based on dynamic voltage restorers (BFCL-DVR) [28]. Another popular bridge topology uses a series connected reactor and high impedance resistor placed inside the diode bridge [18], [19]. The resistor can be bypassed by an IGBT switch for suppressing the fault current. This topology has extended versions with high impedance in parallel to the bridge [20], [21], [22], [23], [24], [25]. Recent works indicate that implementation of active bridge FCL [29], [30], [31], [32], [33] results in better enhancement of wind turbine transients stability than SDBR [15], [34].

This paper presents a new topology of active bridge FCL with switched limiting impedance, that is comprised of only a reactor and resistor. This work is motivated by a series of recent works on active bridge FCLs shown in [18], [19], [30], [31], in which, during normal operation, the IGBT switch bypasses only the limiting resistor. The active bridge FCL proposed in these articles poses two major drawbacks during normal operation, which are increased power losses on the reactor's internal resistance, and harmonic distortion in the line current. To address these drawbacks, the proposed FCL completely removes the limiting impedance from the circuit during normal operation. As a result, the proposed FCL topology eliminates power losses in the reactor internal resistor, reduces harmonic distortion in the line current, and provides better transient stability of the wind farm. The proposed FCL is compared to the classic diode bridge, SDBR, and active diode bridge FCL circuits. The comparison is done using a benchmark system that includes a 9 MW wind turbine with a doubly fed induction generator (DFIG), two 50 MW synchronous generators, and three step-up transformers. The results show that all three FCLs improve transient stability by limiting the currents peak, terminal voltage drop, active and reactive powers, and torque transients.

The paper is organized as follows. Section II presents the operation principles. The proposed fault current limiter is shown in Section III. Section IV explains the structure of DFIG wind turbine. The numeric results are discussed in Section V.

The work of Y. Levron was partly supported by Israel Science Foundation grant No. 1227/18. D. Baimel is with Shamoon College of Engineering, Beer-Sheva 84100, Israel (e-mail of corresponding author: baimel@post.bgu.ac.il). N. Roy Chowdhury and Y. Levron are with the Andrew and Erna Viterbi Faculty of Electrical Engineering, Technion—Israel Institute of Technology, Haifa, 3200003, Israel (emails: nilanjan2008@gmail.com, yoashl@ee.technion.ac.il). J. Belikov is with the Department of Software Science, Tallinn University of Technology, Akadeemia tee 15a, 12618 Tallinn (email: juri.belikov@taltech.ee).

Paper submitted to the International Conference on Power Systems Transients (IPST 2021) in Belo Horizonte, Brazil June 6–10, 2021.

II. Operation Principle of Conventional Diode Bridge, SDBR and Active Diode Bridge FCLs

A. Conventional Diode Bridge FCL

Figure 1 shows the conventional bridge type FCL, which is comprised of a diode bridge and reactor L_d with internal resistance R_d, where Z_F denotes fault impedance and Z_{load} is the load impedance [13], [16], [17]. During normal operation and steady state, the inductor is charged to the peak value of the line current so that the current is approximately constant and the voltage drop across the reactor tends to zero.

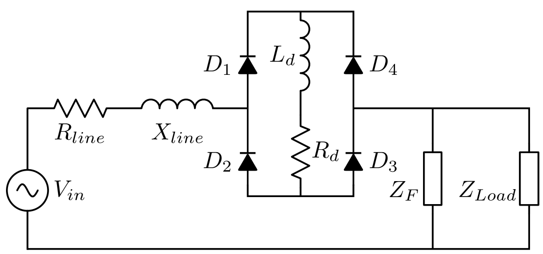

Fig. 1. Conventional diode bridge FCL.

During a fault, the current is limited by the impedance of the reactor L_d, so the fault current will increase during the fault period gradually. The amplitude of the fault current depends on the value of the reactor's inductance. Furthermore, the DC reactor limits a sudden rise of fault current, this instantaneously preventing sudden voltage drop at machine terminal and improving transient behavior.

The main advantages of this FCL is simple structure and absence of a controller. The disadvantage is that after several 50/60 Hz cycles, the reactor is charged to the fault current and its effect on the transient stability reduces.

B. Series Dynamic Breaking Resistor

The principle operation scheme of the SDBR is shown in Fig. 2 [15], [34]. During normal operation, the bypass switch is closed and the breaking resistor is bypassed. The bypass switch can be implemented by mechanical switch or semicoductor, i.e. IGBT.

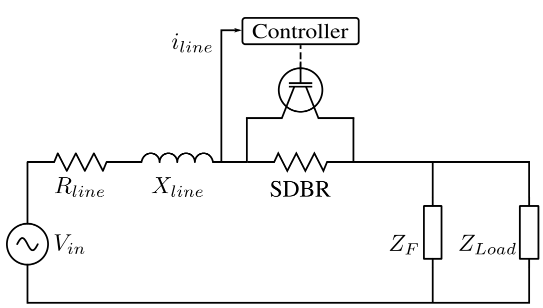

Fig. 2. Series dynamic breaking resistor.

During fault operation, the switch is opened and the breaking resistor limits the fault current and the energy is dissipated in the resistor, raising its temperature. Therefore, it is important to choose the resistor according to its temperature and the maximum energy dissipation limits.

C. Active Diode Bridge

The studied active diode bridge FCL was already mentioned in the literature and it is a combination of the conventional diode bridge FCL and SDBR [18], [19]. Its main advantages are simple structure and control, cost effectiveness and high capability to limit the fault currents and suppress transients. The disadvantages are power losses associated with reactor's internal resistance R_d, more complicated structure and control compared to conventional diode bridge and SDBR. Additional disadvantage present during normal operation is the presence of the reactor inside the bridge results in two operation modes (charging and freewheeling) that leads to harmonic distortion of the line current. Additional example of another active diode bridge FCL is shown in [21].

The presented active diode bridge FCL is comprised of four diodes that form passive rectifier with series connected reactor L_d that has internal resistance R_d and high impedance resistor R, which is connected in parallel with the fast response semi-conductor IGBT switch, as shown in Fig. 3.

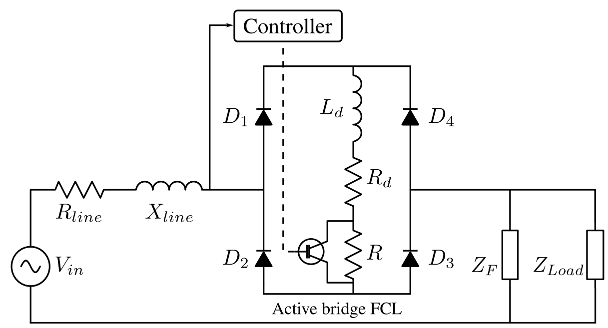

Fig. 3. Active diode bridge FCL.

During the normal operation, the IGBT switch is closed so that resistor is bypassed and FCL operates as conventional diode bridge FCL without effecting the power system. In case of fault, the reactor limits a sudden rise of fault current. When the line current reaches predefined threshold value, the IGBT switch is opened so that resistor R is added to the fault current path. Consequently, high impedance comprised of reactor's L_d reactance and resistance R limits the fault current and resistor R consumes the excess of energy from the DFIG, helping to ensure system transient stability.

III. Proposed Bridge FCL

The proposed FCL, shown in Figure 4, is an improved version of the popular active diode bridge FCL topology that was explained in previous subsection and discussed in [18], [19], [30], [31]. The proposed FCL aims to overcome the drawbacks associated with active diode bridge FCL while preserving its advantages. In the active bridge FCL topology, the bypass IGBT is connected in parallel with resistor R so that the current flows through the reactor in both normal and fault operation modes. Therefore, during normal operation, there are power losses associated with reactor's internal resistance R_d and harmonic distortion of the line current due to the charging and freewheeling modes. Furthermore, the DC reactor is charged to the maximum value of the load current during normal operation. Therefore, when the fault starts, the reactor's initial current is maximum value of the load current so its limiting capability of the rising fault current is reduced. The improvement of the proposed FCL is connection of the bypass IGBT in parallel with both reactor L_d and resistor R so that during normal operation mode, when the IGBT switch is closed, the reactor and resistor are bypassed and rectified sinusoidal current flows through the bridge. Therefore, during normal operation, the power losses on resistor R_d and harmonic distortion of the line current are avoided. During the fault period, when the line current rises above threshold value of the current, the controller opens IGBT switch so that reactor L_d and resistor R are added to the fault current path and limit the fault current. The reactor is charged from zero so it has better limiting capability of the rising fault current than standard active diode bridge FCL. This results in better transient stability of the wind farm, as will be shown later. It is important to note that the main advantages of the active bridge FCL which are simple structure and control are preserved in the proposed topology. The components of FCL and its control principle remain the same as in active bridge FCL. The drawback of the proposed FCL compared to previously presented active diode bridge FCL is that the fault current rise rate will not be limited until the controller identifies the fault current and opens IGBT. However, typical response time of IGBT is 150[nsec] so that the damage that can be caused by the fault current during that time is limited. This drawback can be further reduced by implementation of a more accurate control and defining lower threshold values for identification of the fault current.

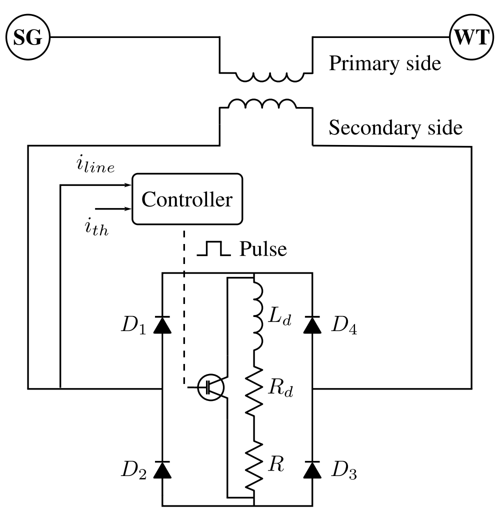

Fig. 4. The proposed active diode bridge FCL (one phase representation).

The fault period can be divided into two operation modes: charging and freewheeling.

A. Charging mode

In this mode, the positive or negative current flows through the transmission line, corresponding pair of diodes, reactor L_d, resistors R_d and R, and short circuit impedance in parallel with load. Therefore, the impedance of the fault circuit during the charging mode is given by

$$\begin{aligned} Z_{SC_{ch}} &= R_{line} + jX_{line} + jX_{L_{DC}} + \\ &+ \frac{(R_F + jX_F)(R_{Load} + jX_{Load})}{(R_F + R_{Load}) + j(X_F + jX_{Load})} \\ &= R_{SC_{ch}} + jX_{SC_{ch}}, \end{aligned} \tag{1}$$

where R_F and X_F are resistance and reactance of the short circuit impedance and R_{Load} and X_{Load} are resistance and reactance of the load. The modulus $|Z_{SC_{ch}}|$ and the angle $\theta_{SC_{ch}}$ of the fault circuit impedance are calculated by

$$|Z_{SC_{ch}}| = \sqrt{R_{SC_{ch}}^2 + X_{SC_{ch}}^2}, \tag{2}$$

$$\theta_{SC_{ch}} = \arctan\left(\frac{X_{SC_{ch}}}{R_{SC_{ch}}}\right). \tag{3}$$

During the positive voltage half cycle, the diodes D_1, D_3 are conducting and during negative half cycle, the diodes D_2, D_2 are conducting. When the fault operation starts, the FCL enters transient state. During the first half cycle, the reactor is charged from zero to the maximum value of the limited current that is defined by the fault circuit impedance $Z_{SC_{ch}}$. In the following half cycles, the FCL enters steady state mode. The charging mode starts when the limited current becomes higher than the reactor current and ends when the limited current becomes smaller than the reactor current. Figure 5 shows the scheme of the power system during the charging mode.

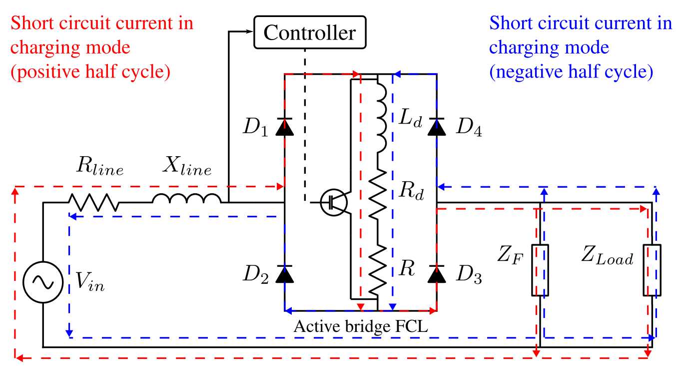

Fig. 5. Charging mode during short circuit to ground (one phase representation).

The voltages in the fault charging mode circuit can be described by

$$V_{in} = R_{SC_{ch}} i_{SC_{ch}} + L_{SC_{ch}} \frac{\mathrm{d} i_{SC_{ch}}}{\mathrm{d}t} + 2V_{DF}, \tag{4}$$

where supply voltage is defined as $V_{in} = \sqrt{2}V_m \sin\omega t$ and V_{DF} is the voltage drop on the diodes.

Solving (4) leads to expression of the short circuit current during the charging mode

$$\begin{aligned} i_{SC_{ch}}(t) &= e^{-\frac{R_{SC_{ch}}}{X_{SC_{ch}}/\omega}(t-t_0)} \Big[i_{SC_{ch}(I.C.)} \\ &- \frac{\sqrt{2}V_m \sin(\omega t_0 - \theta_{SC_{ch}})}{|Z_{SC_{ch}}|} + \\ &+ \frac{2V_{DF}}{R_{SC_{ch}}} \Big] + \frac{\sqrt{2}V_m \sin(\omega t - \theta_{SC_{ch}})}{|Z_{SC_{ch}}|} - \frac{2V_{DF}}{R_{SC_{ch}}}, \end{aligned} \tag{5}$$

where $i_{SC_{ch}(I.C.)}$ is the initial condition of the reactor charging current and t_0 is the starting time of the charging mode.

B. Freewheeling mode

Figure 6 shows the operation principle of the proposed FCL in the freewheeling mode. After reaching its maximum value, the reactor current begins to decrease and the polarity of the voltage drop across reactor L_d reverses. Once its absolute value exceeds $2V_{DF}$, the two previously non-conducting diodes are turned ON; this is in addition to the two diodes that were already conducting, i.e., all four diodes conduct and the freewheeling mode starts. The reactor L_d freewheels, discharging through all four diodes.

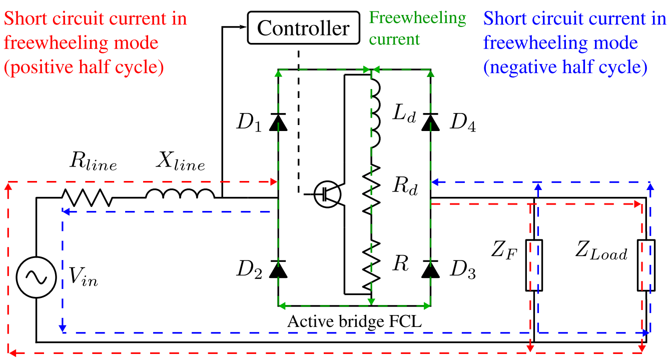

Fig. 6. Freewheeling mode during short circuit to ground (one phase representation).

The fault impedance in the freewheeling mode is given by

$$\begin{aligned} Z_{SC_{fw}} &= R_{line} + jX_{line} \\ &+ \frac{(R_F + jX_F)(R_{Load} + jX_{Load})}{(R_F + R_{Load}) + j(X_F + jX_{Load})} \\ &= R_{SC_{fw}} + jX_{SC_{fw}}, \end{aligned} \tag{6}$$

The voltages' equation during fault freewheeling mode

$$V_{in} = R_{SC_{fw}} i_{SC_{fw}} + L_{SC_{fw}} \frac{di_{SC_{fw}}}{dt} + 2V_{DF} \tag{7}$$

allows calculation of the short circuit current $i_{SC_{fw}}$ during the freewheeling mode

$$\begin{aligned} i_{SC_f w}(t) = e^{-\frac{R_{SC_{fw}}}{X_{SC_{fw}}/\omega}(t-t_1)} \Big[& i_{SC_f w(I.C.)} - \\ & - \frac{\sqrt{2}V_m \sin(\omega t_1 - \theta_{SC_{fw}})}{|Z_{SC_{fw}}|} \Big] \\ & + \frac{\sqrt{2}V_m \sin(\omega t - \theta_{SC_{fw}})}{|Z_{SC_{fw}}|}, \end{aligned} \tag{8}$$

where $i_{SC_{fw}(I.C.)}$ is the initial condition of the freewheeling current and t_1 is the time point at which the charging mode ends and the freewheeling mode starts.

The reactor current $i_{L_D}(t)$ is given by

$$i_{L_D}(t) = i_{SC_{ch}}(t_1) - \frac{2V_{DF}}{L_D} t. \tag{9}$$

IV. Wind Turbine Model

The model of wind DFIG turbine with rotor-side (RSC) and grid-side (GSC) converters is shown in Fig. 7. These converters are based on voltage source converter (VSC) and can convert active and reactive powers in both directions (AC/DC/AC). The converters are connected through DC-link capacitor that reduces DC voltage ripple within a small defined range. The rotor-side converter typically controls the real and reactive power of the induction machine while the grid-side converter controls the DC-link voltage and power factor. These converters are controlled independently by the $dq0$ vector control approach [35].

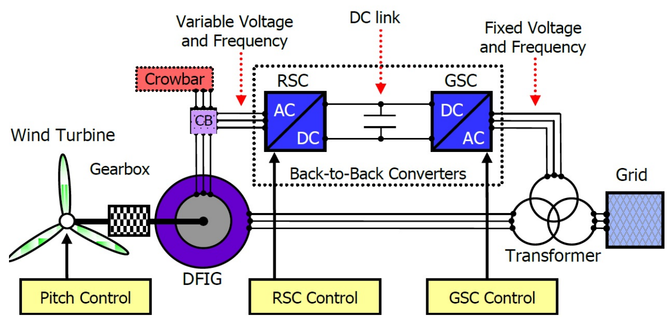

Fig. 7. The model of wind DFIG turbine.

The mechanical output power of the wind turbine is

$$P_w = \frac{1}{2}\pi\rho R^2 V_\omega^3 C_p(\lambda, \beta), \tag{10}$$

where ρ is the air density, R is the blade radius, V_w is the wind velocity, and C_p is the power coefficient that depends on tip speed ratio λ and blade pitch angle β. The tip speed ratio λ can be calculated by

$$\lambda = \frac{\omega_r R}{V_\omega}, \tag{11}$$

and the power coefficient C_p is given by

$$C_p(\lambda, \beta) = \frac{1}{2}(\lambda - 0.022\beta - 5.6). \tag{12}$$

Typical parameters of DFIG machines are explained in Table I, where subscripts d, q, s, r denote the dq components of the stator and rotor, respectively.

TABLE I
Nomenclature: Induction Machine

Parameter	Physical meaning
$v_{d,s}$, $v_{q,s}$, $v_{d,r}$, $v_{q,r}$	voltages
$i_{d,s}$, $i_{q,s}$, $i_{d,r}$, $i_{q,r}$	currents
$\phi_{d,s}$, $\phi_{q,s}$, $\phi_{d,r}$, $\phi_{q,r}$	fluxes
R_s, R_r	winding resistances
L_s, L_r	self-inductances
$L_{l,s}$, $L_{l,r}$	leakage inductances
L_{sr}	stator to rotor mutual inductance
L_m	magnetizing inductance

The voltage equations of DFIG in the dq reference frame are given by [36]

$$\begin{aligned} v_{d,s} &= R_s i_{d,s} + \frac{\mathrm{d}}{\mathrm{d}t}\phi_{d,s} - \omega_s \phi_{q,s}, \\ v_{q,s} &= R_s i_{q,s} + \frac{\mathrm{d}}{\mathrm{d}t}\phi_{q,s} + \omega_s \phi_{d,s}, \\ v_{d,r} &= R_r i_{d,r} + \frac{\mathrm{d}}{\mathrm{d}t}\phi_{d,r} - (\omega_s - \omega_r)\,\phi_{q,r}, \\ v_{q,r} &= R_r i_{q,r} + \frac{\mathrm{d}}{\mathrm{d}t}\phi_{q,r} + (\omega_s - \omega_r)\,\phi_{d,r}, \end{aligned} \tag{13}$$

where ω_s is the nominal system frequency, ω_r denotes angular velocity of the rotor, and flux equations are given by

$$\begin{aligned} \phi_{d,s} &= L_s i_{d,s} + L_{sr} i_{d,r} = (L_{l,s} + L_m)\, i_{d,s} + L_{sr} i_{d,r}, \\ \phi_{q,s} &= L_s i_{q,s} + L_{sr} i_{q,r} = (L_{l,s} + L_m)\, i_{q,s} + L_{sr} i_{q,r}, \\ \phi_{d,r} &= L_r i_{d,r} + L_{sr} i_{d,s} = (L_{l,r} + L_m)\, i_{d,r} + L_{sr} i_{d,s}, \\ \phi_{q,r} &= L_r i_{q,r} + L_{sr} i_{q,s} = (L_{l,r} + L_m)\, i_{q,r} + L_{sr} i_{q,s}. \end{aligned} \tag{14}$$

V. Numeric Results

Figure 8 shows one line diagram of the tested power system. This system represents part of power grid that has 9MW DFIG wind farm comprised of six parallel connected 1.5MW DFIG wind turbines, two 50MW synchronous generators, three step-up transformers that raise wind farm's and generators' voltage up to 25kV, and 200kW/10kVAR power load. Generators 1 and 2, wind farm and load are connected at Point of Common Coupling (PCC) and located at 30km, 15km, 5km, 15km from PCC, respectively.

During normal and steady state operations of the power system, at time point 0.4s, starts three phase short circuit fault that is located at power line that feeds the load, as shown in Fig. 8. As a result, the circuit breaker is tripped after 30ms delay during which the short circuit current can cause significant damage to the power system, while transient processes may increase system instability. In order to analyze how the use of FCLs can decrease the influence of this fault on the transient stability of the DFIG wind farm, the tested FCLs are located at the output of the wind farm, at the step up substation of the wind farm. The five studied operation cases are absence of FCL, conventional diode bridge FCL, SDBR, active diode bridge FCl and proposed FCL.

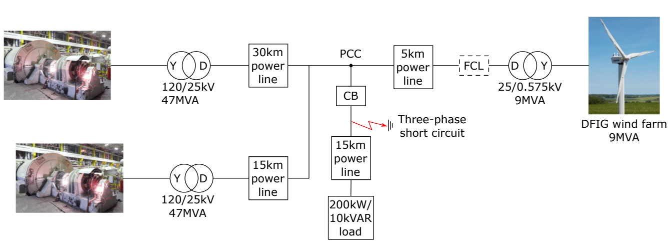

Fig. 8. Tested power system.

The simulations were performed by using MATLAB/Simulink software. The three phase fault starts at 0.4sec and removed at 0.43sec by tripping the corresponding circuit breaker. In order to avoid undesirable power losses on SDBR breaking resistor and active diode bridge FCL's series resistor, they are removed from the circuit after opening the circuit breaker by turning ON parallel IGBTs. Therefore, the analysis of the simulated parameters is divided into two periods. The first, fault period is defined for $t_f \in [0.4, 0.43]$. The second, restoration period, takes place after tripping the circuit breaker at $t = 0.43$. The analysis and comparison of studied cases during the fault and restoration periods are summarized in Table II. This comparison relies on the evaluation indexes of transient stability for each parameter, which are based on integration of parameters' deviation from their nominal values. The evaluation indexes are defined by

$$p_{index} = \int_{t_s}^{t_e} |\Delta p|\, \mathrm{d}t, \tag{15}$$

where p stands for the corresponding parameter, i.e. current, voltage, active and reactive powers and torque, t_s and t_e stand for the time points at which the fault or the restoration periods begin and end, respectively. According to (15), higher value of the evaluation index means lower transient stability of the corresponding parameter and vice versa. Examination of Table II shows that implementation of the proposed FCL results in significant improvement of transient stability of current, voltage, active power and torque during fault current period. During restoration period the proposed FCL improves transient stability of voltage, active, and reactive power.

TABLE II
Analysis and Comparison of Transient Stability Improvement of Wind Turbine Parameters in Different Case Studies

Parameter (TSI)	Period	Without FCL	Diode bridge	SDBR	Active diode bridge	Proposed FCL
Current	Fault	3	1.88	1.25	0.82	0.42
Current	Restoration	1.63	1.3	0.95	1.06	1.07
Voltage	Fault	2.11	1.83	1.35	1.13	0.46
Voltage	Restoration	1.02	1.05	0.84	0.64	0.56
Active power	Fault	1.65	1.3	0.69	0.65	0.11
Active power	Restoration	2.9	3.1	2	1.47	0.8
Reactive power	Fault	0.55	0.45	0.35	0.46	0.66
Reactive power	Restoration	1.35	2.35	3.16	3.12	1.9
Torque	Fault	2.17	2.77	1.44	1.46	0.56
Torque	Restoration	2.89	3.38	1.29	0.84	2

The parameters of the simulated wind turbine, DFIG, and three types of compared FCls are shown in Table III. The wind speed is set to 15m/s.

TABLE III
SIMULATION PARAMETERS OF THE WIND TURBINE, DFIG AND DISCUSSED FCLS

Parameter	Value	Units
Nominal mechanical output power	1.5	MW
Stator nominal voltage	575	V
Frequency	60	Hz
Stator leakage resistance	0.023	pu
Stator leakage inductance	0.18	pu
Rotor leakage resistance	0.016	pu
Rotor leakage inductance	0.16	pu
Magnetizing inductance	2.9	pu
Inertia constant	0.685	–
Friction factor	0.1	–
Pole pairs	3	–
Nominal DC bus voltage	1150	V
DC bus capacitor	0.01	F
Reactor inductance L_d	1	H
Reactor internal resistance R_d	1	Ω
Series resistance R and SDBR	99	Ω
Threshold current value for turning IGBT Off	1.07	*pu*
Threshold current value for turning IGBT On	0.8	*pu*

Following figures show simulation results of DFIG wind farm transient behavior for five studied cases during three phase fault.

Figure 9 shows the fault current i_{WT} measured at the terminals of the wind farm. During the fault period $t \in [0.4, 0.43]$ the best results are achieved for the proposed FCL. During time period $t_1 \in [0.4, 0.42]$, the proposed FCL limits the fault current to $i_{WT} < 1$pu while during $t_2 \in [0.42, 0.43]$, the limited fault current rises to $i_{WT} = 1.09$pu. The active bridge FCL limits the current to $i_{WT} = 1.32$pu while without FCL, the current reaches $i_{WT} = 2.39$pu. When conventional diode bridge FCL is used, the current is suppressed to $i_{WT} = 1.943$pu while SDBR reduces the current to $i_{WT} = 1.54$pu. However, the situation is different during the restoration period defined between $t \in [0.43, 0.5]$. In terms of transient stability, the fluctuations are almost similar for all cases but in terms of current amplitude peak, the performance the proposed FCL is better than active diode bridge FCL but worse than other cases. This is due to the transients related to the series reactor inside the bridge.

Figure 10 shows that without FCL, the DFIG terminal voltage v_{WT} drops almost to zero right after the fault begins. This abrupt voltage drop creates stress on the system particularly on the induction machine. The voltage drop improves after inserting series FCL into the system. The conventional diode bridge FCL improves voltage drop only in the time interval of $t \in [0.42, 0.423]$ after which the voltage drop becomes equal to the voltage drop without FCL. This is explained by the fact that reactor is gradually charged to the fault current and its influence on the voltage drop reduces. The SDBR provides lower voltage drop than conventional diode bridge FCL so that the voltage drop is limited to to $v_{WT} = 0.26$pu while active diode bridge FCL results voltage drops only to $v_{WT} = 0.4$pu. The lowest voltage drop of $v_{WT} = 0.58$pu is achieved with the proposed FCL. During the restoration period, after fault recovery, the terminal voltage returns to the pre-fault level.

Figure 11 shows generator active power P_{WT} response. During the fault period, the DFIG output active power drops almost to zero. The conventional diode bridge FCL improves active power drop only in the time interval $t \in [0.42, 0.423]$ after which the active power drop becomes equal to the power drop without FCL. It is interesting to note that active diode bridge FCL and SDBR reduce the power drop almost equally to $P_{WT} = 0.4$pu. The best results are obtained for the proposed FCL with active power drop to $P_{WT} = 0.6$pu. During the restoration period, the proposed FCL, active diode bridge FCL and SDBR have faster recovery than conventional diode bridge FCL.

Figure 12 shows that during fault period, reactive power (Q_{WT}) consumed from the wind farm rises from 0 to 0.63pu. This power spike is limited by using conventional diode bridge FCL or proposed FCL to $Q_{WT} = 0.42$pu. Implementation of active diode bridge FCL and SDBR reduce this rise to $Q_{WT} = 0.27$pu so their performance is almost similar. During the restoration period the situation is reversed. The DFIG draws high reactive power so that highest negative reactive power peak of $Q_{WT} = -1.15$pu is obtained for active diode bridge FCL case. Smaller negative reactive power peak of $Q_{WT} = -0.97$pu is obtained for SDBR and proposed FCL. In the case of conventional diode bridge FCL, the obtained negative reactive power is $Q_{WT} = -0.8$pu while the lowest power peak of $Q_{WT} = -0.73$pu is obtained without FCL.

Figure 13 shows the DFIG electrical torque behavior. The fault causes significant fluctuation in electrical torque. These quick and large changes in torque are harmful for the wind turbine generator system. The integration of conventional diode bridge FCL slightly reduces the fluctuations but it is not good enough. The best results are achieved by using proposed FCL that provides better and quicker stabilization. During the restoration period, the lowest fluctuations were obtained for SDBR case.

Figure 14 compares three rectified currents that flow through the DC path of the conventional diode, active bridge and proposed FCLs. During the normal operation period $t \in [0, 0.4]$, the rectified current of the conventional and active diode bridge flows through reactor L_d, that is charged to the maximum value of the line current 55A. The rectified current of the proposed FCL flows through IGBT switch and therefore, it has rectified sine waveform. During the fault period $t \in [0.4, 0.43]$, the reactor of the conventional diode bridge FCL is charged to the maximum transient value of the limited short circuit current 125A. In the active diode bridge and proposed FCLs, the peak values of rectified currents are smaller than in conventional diode bridge FCL (up to 86A) and have ripple around 30A. During the restoration period $t \in [0.43, 0.5]$, the rectified current of the conventional diode bridge FCL remains almost constant. In the active diode bridge FCL, the reactor is charged to the maximum value of the transient current 94A. In the proposed FCL, after transient spike, the rectified current returns to the rectified sinusoidal form. It is important to note that this transient spike results in 18.5kV voltage which is below nominal voltage value 25kV.

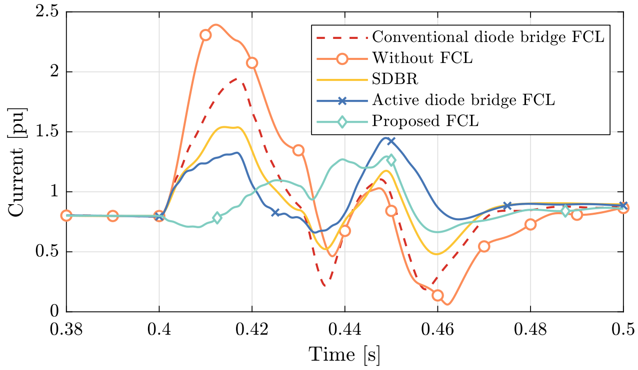

Fig. 9. Current at the wind farm terminals.

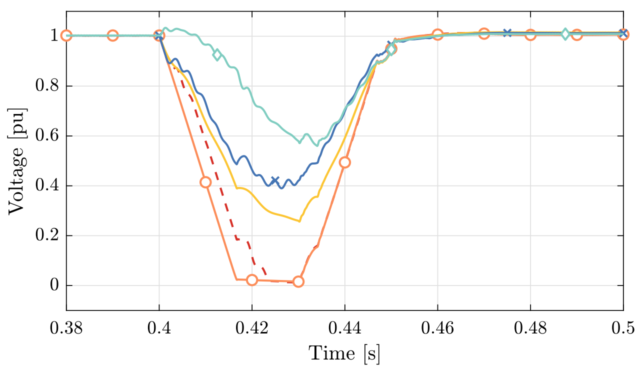

Fig. 10. Voltage at the wind farm terminals.

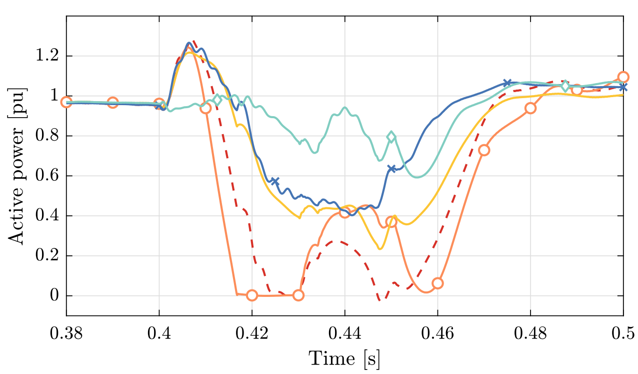

Fig. 11. Active power of the wind farm.

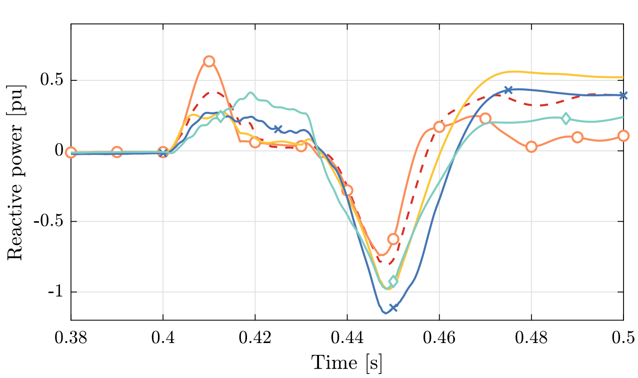

Fig. 12. Reactive power of the wind farm.

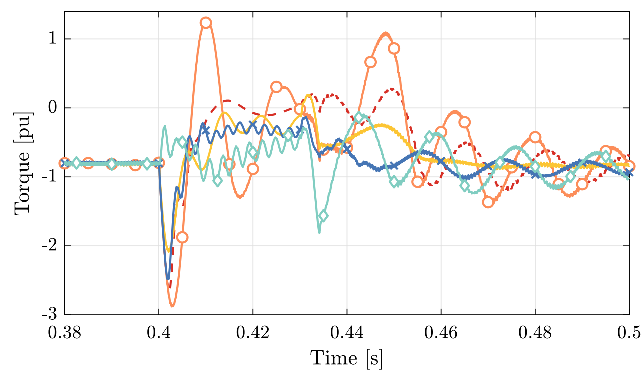

Fig. 13. Torque of the wind turbine.

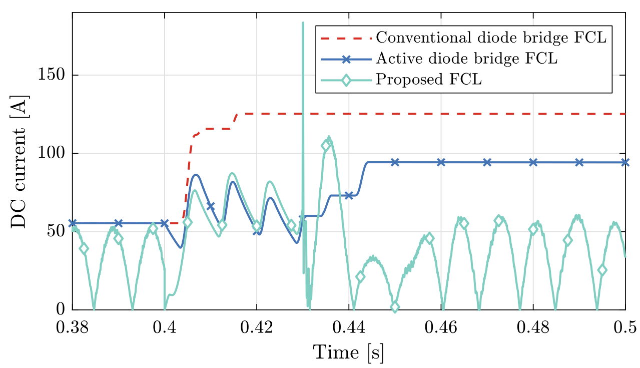

Fig. 14. The rectified currents that flow through the DC path of the conventional diode, active and proposed bridge FCLs.

In addition to the transient stability enhancement of the DFIG wind farm, the discussed types of FCLs also improve THD of fault voltages and currents at the wind farm terminals. During normal operation, the voltage THD is 2.8% while current THD is 1.4%, which is in compliance with IEEE standard (519) that limits harmonic current and voltage injection. However, during the fault, significant amount of harmonics are injected into the PCC. Table IV shows how each type of FCL influences the THD of voltages and currents at the wind farm terminals. Examination of Table IV shows that conventional diode bridge FCL is not effective in harmonics suppression. However, SDBR and active diode bridge FCL significantly improve THD of both current and voltage, while the best THD results are achieved with proposed FCL.

TABLE IV
COMPARISON OF THD VALUES OF FAULT VOLTAGES AND CURRENTS FOR DIFFERENT TYPES OF FCLS

FCL	Current THD %	Voltage THD %
Diode bridge FCL	81	218
Without FCL	88	179
SDBR bridge FCL	54	129
Active bridge FCL	45	77
Proposed active bridge FCL	38.3	41.1

VI. CONCLUSIONS

This paper presents a new FCL topology that during normal operation ensures reduced power losses, reduces THD of the load current and improved DFIG wind farm transient stability. It is shown that during the fault all tested FCLs have improved transient stability by limiting current peaks, voltage drop, active and reactive powers, and torque transients. Using SDBR resulted in moderate transient enhancement. The active diode bridge FCL and SDBR provided almost equal results in reduction of active and reactive power and torque transients, with slightly better performance of the active bridge. The worst results for all discussed parameters were obtained with conventional diode bridge FCL. Harmonics analysis showed that the proposed FCL ensured better harmonics suppression in wind farm fault currents and voltages than other cases. However, during the restoration period the situation is changed. Current transient stability is moderate for the proposed FCL and poor for active diode bridge FCL. Furthermore, the best transient stability of reactive power was achieved without FCLs while the worst results were obtained with active diode bridge FCL case. Torque transient stability also got worse for all cases except SDBR that has provided best transient stability for this period. Therefore, using FCLs may have unexpected negative impact on transient stability of the wind farm during restoration period. This conclusion should be taken into account during design and analysis of power systems containing DFIG wind farms.

References

[1] J. Vidal, G. Abad, J. Arza, and S. Aurtenechea, "Single-phase DC crowbar topologies for low voltage ride through fulfillment of high-power doubly fed induction generator-based wind turbines," *IEEE Transactions on Energy Conversion*, vol. 28, no. 3, pp. 768–781, 2013.

[2] A. Safaei, M. Zolfaghari, M. Gilvanejad, and G. B. Gharehpetian, "A survey on fault current limiters: Development and technical aspects," *International Journal of Electrical Power & Energy Systems*, vol. 118, p. 105729, 2020.

[3] H.-C. Jo and S.-K. Joo, "Superconducting fault current limiter placement for power system protection using the minimax regret criterion," *IEEE Transactions on Applied Superconductivity*, vol. 25, no. 3, pp. 1–5, 2015.

[4] S. M. Blair, C. D. Booth, I. M. Elders, N. K. Singh, G. M. Burt, and J. McCarthy, "Superconducting fault current limiter application in a power-dense marine electrical system," *IET Electrical Systems in Transportation*, vol. 1, no. 3, pp. 93–102, 2011.

[5] M. T. Hagh and M. Abapour, "Nonsuperconducting fault current limiter with controlling the magnitudes of fault currents," *IEEE Transactions on Power Electronics*, vol. 24, no. 3, pp. 613–619, 2009.

[6] N. Hayakawa, K. Ishida, M. Mimbu, H. Kojima, S. Isojima, and M. Kuwata, "Volume effect of dynamic breakdown strength in LN2 for insulation design of resistive superconducting fault current limiters," *IEEE Transactions on Applied Superconductivity*, vol. 28, no. 4, pp. 1–4, 2018.

[7] H. Ge, K. Yang, M. Junaid, Y. Tan, Z. Liu, Y. Geng, and J. Wang, "A quenching recovery time test method for resistive type superconducting fault current limiters used in DC circuit," in *4th International Conference on Electric Power Equipment-Switching Technology (ICEPE-ST)*. IEEE, 2017, pp. 393–396.

[8] L. Chen, X. Zhang, Y. Qin, H. Chen, Q. Shen, Y. Xu, L. Ren, and Y. Tang, "Application and design of a resistive-type superconducting fault current limiter for efficient protection of a DC microgrid," *IEEE Transactions on Applied Superconductivity*, vol. 29, no. 2, pp. 1–7, 2018.

[9] D. Qiu, Z. Li, F. Gu, Z. Huang, A. Zhao, D. Hu, B. Wei, H. Huang, Z. Hong, K. Ryu *et al.*, "Experiment study on an inductive superconducting fault current limiter using no-insulation coils," *Physica C: Superconductivity and its Applications*, vol. 546, pp. 1–5, 2018.

[10] Y. Dong, J. Zhu, D. Wei, W. Chen, Q. Du, K. Zhang, P. Chen, K. Lu, H. Jiang, S. Wang *et al.*, "10 kV AC test verification of the high temperature superconducting fault current limiter with bias magnetic field," *Cryogenics*, vol. 112, p. 103195, 2020.

[11] X.-Y. Xiao, R.-H. Yang, X.-Y. Chen, and Z.-X. Zheng, "Integrated DFIG protection with a modified SMES-FCL under symmetrical and asymmetrical faults," *IEEE Transactions on Applied Superconductivity*, vol. 28, no. 4, pp. 1–6, 2018.

[12] M. E. Elshiekh, D.-E. A. Mansour, M. Zhang, W. Yuan, H. Wang, and M. Xie, "New technique for using SMES to limit fault currents in wind farm power systems," *IEEE Transactions on Applied Superconductivity*, vol. 28, no. 4, pp. 1–5, 2018.

[13] M. Firouzi, G. B. Gharehpetian, and B. Mozafari, "Bridge-type superconducting fault current limiter effect on distance relay characteristics," *International Journal of Electrical Power & Energy Systems*, vol. 68, pp. 115–122, 2015.

[14] K. E. Okedu, S. M. Muyeen, R. Takahashi, and J. Tamura, "Improvement of fault ride through capability of wind farms using DFIG considering SDBR," in *14th European Conference on Power Electronics and Applications*. IEEE, 2011, pp. 1–10.

[15] S. M. Muyeen, "A combined approach of using an SDBR and a STATCOM to enhance the stability of a wind farm," *IEEE Systems Journal*, vol. 9, no. 3, pp. 922–932, 2014.

[16] H. J. Boenig, C. H. Mielke, B. L. Burley, H. Chen, J. A. Waynert, and J. O. Willis, "The bridge-type fault current controller-a new FACTS controller," in *IEEE Power Engineering Society Summer Meeting*, vol. 1. IEEE, 2002, pp. 455–460.

[17] K. M. Salim, T. Hoshino, A. Kawasaki, I. Muta, and T. Nakamura, "Waveform analysis of the bridge type SFCL during load changing and fault time," *IEEE Transactions on Applied Superconductivity*, vol. 13, no. 2, pp. 1992–1995, 2003.

[18] S. B. Naderi, M. Jafari, and M. T. Hagh, "Controllable resistive type fault current limiter (CR-FCL) with frequency and pulse duty-cycle," *International Journal of Electrical Power & Energy Systems*, vol. 61, pp. 11–19, 2014.

[19] U. Chaudhary, P. Tripathy, and S. K. Nayak, "Application of bridge-type FCL for betterment of FRT capability for dfig-based wind turbine," in *IEEE Power India International Conference*. IEEE, 2014, pp. 1–6.

[20] H. Bahramian-Habil, A. H. Askarian, and G. B. Gharehpetian, "Improving LVRT capability of microgrid by using bridge-type fault current limiter," *Electric Power Systems Research*, vol. 191, p. 106872, 2021.

[21] M. A. H. Sadi and M. H. Ali, "Transient stability enhancement by bridge type fault current limiter considering coordination with optimal reclosing of circuit breakers," *Electric Power Systems Research*, vol. 124, pp. 160–172, 2015.

[22] M. A. Shobug and M. R. I. Sheikh, "Fault management in DFIG based wind turbine using sophisticated advanced solid state fault current limiter," in *IEEE Region 10 Symposium (TENSYMP)*. IEEE, 2020, pp. 1660–1663.

[23] M. S. Alam, A. Hussein, M. A. Abido, and Z. M. Al-Hamouz, "VSC-HVDC system stability augmentation with bridge type fault current limiter," in *6th International Conference on Clean Electrical Power (ICCEP)*. IEEE, 2017, pp. 531–535.

[24] A. Mokarim, B. Dwivedi, and P. Verma, "Comparative study of different bridge fault current limiters applied in doubly fed induction generator for improvement of fault ride-through capability," in *International Conference on Automation, Computational and Technology Management (ICACTM)*, 2019, pp. 256–261.

[25] M. R. Islam, J. Hasan, M. N. Huda, and M. A. H. Sadi, "Fault ride through capability improvement of DFIG based wind farms using active power controlled bridge type fault current limiter," in *North American Power Symposium (NAPS)*. IEEE, 2019, pp. 1–6.

[26] P. Kumar and P. Shaw, "Comparison of superconducting fault current limiter topologies based on power electronic devices," in *7th India International Conference on Power Electronics (IICPE)*. IEEE, 2016, pp. 1–5.

[27] L. Wei, B. Chen, and J. Yuan, "Limiting mechanism and equivalent analytical model of a bridge-type saturated core fault current limiter," *Electric Power Systems Research*, vol. 180, p. 106134, 2020.

[28] C. Tu, Q. Guo, F. Jiang, Z. Shuai, and X. He, "Analysis and control of bridge-type fault current limiter integrated with the dynamic voltage restorer," *International Journal of Electrical Power & Energy Systems*, vol. 95, pp. 315–326, 2018.

[29] M. E. Hossain, "A non-linear controller based new bridge type fault current limiter for transient stability enhancement of DFIG based wind farm," *Electric Power Systems Research*, vol. 152, pp. 466–484, 2017.

[30] M. I. Marei, H. S. El-Goharey, and R. M. Toukhy, "Fault ride-through enhancement of fixed speed wind turbine using bridge-type fault current limiter," *Journal of Electrical Systems and Information Technology*, vol. 3, no. 1, pp. 119–126, 2016.

[31] P. Techama, S. Polmai, and C. Bunlaksananusorn, "A transformerless multi-cell solid-state fault current limiter for medium voltage power system," in *International Power Electronics Conference (IPEC-Niigata 2018-ECCE Asia)*, 2018, pp. 2490–2495.

[32] M. Firouzi and G. B. Gharehpetian, "LVRT performance enhancement of DFIG-based wind farms by capacitive bridge-type fault current limiter," *IEEE Transactions on Sustainable Energy*, vol. 9, no. 3, pp. 1118–1125, 2017.

[33] M. A. H. Sadi, A. AbuHussein, and M. A. Shoeb, "Transient performance improvement of power systems using fuzzy logic controlled capacitive-bridge type fault current limiter," *IEEE Transactions on Power Systems*, 2020.

[34] A. Causebrook, D. J. Atkinson, and A. G. Jack, "Fault ride-through of large wind farms using series dynamic braking resistors," *IEEE Transactions on Power Systems*, vol. 22, no. 3, pp. 966–975, 2007.

[35] D. Baimel, "Implementation of DQ0 control methods in high power electronics devices for renewable energy sources, energy storage and FACTS," *Sustainable Energy, Grids and Networks*, vol. 18, p. 100218, 2019.

[36] D. Baimel, J. Belikov, J. M. Guerrero, and Y. Levron, "Dynamic modeling of networks, microgrids, and renewable sources in the dq0 reference frame: A survey," *IEEE Access*, vol. 5, pp. 21 323–21 335, 2017.